Journal of Materials Chemistry C

Accepted Manuscript

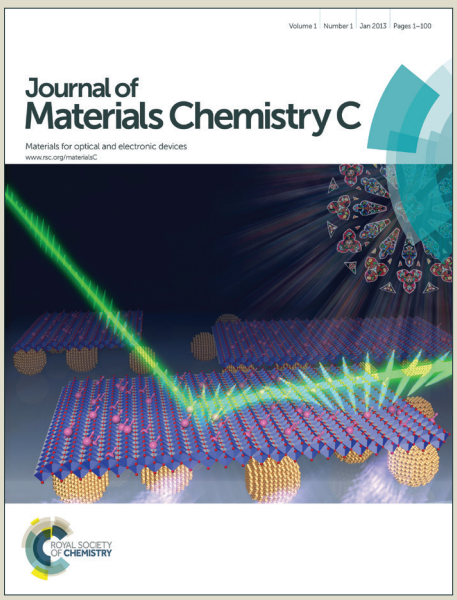

ROYAL SOCIETY OF CHEMISTRY

www.rsc.org/materialsC

The Modulation of Metal-Insulator Transition Temperature of Vanadium Dioxide: A Density Functional Theory Study

Chao Sun [a,b], Liuming Yan [b,*], Baohua Yue [b], Huiting Liu [b], Yanfeng Gao[c]

[(a)] Department of Physics, College of Sciences, [(b)] Department of Chemistry, College of Sciences,

[(c)] School of Materials Science and Engineering, Shanghai University

99 Shangda Road, Shanghai 200444, China

ABSTRACT

The modulation of metal-insulator transition (MIT) temperature and phase stability of thermochromic materials based on all the transition metal doped VO_2 were systematically studied using density functional theory (DFT) calculations. The free energies, formation enthalpies, and Fermi energies of transition metal doped VO_2 were evaluated from DFT calculations, the cell volumes and bulk moduli were obtained by fitting the free energies to the Birch-Murnaghan equation of states, and the decomposition enthalpies and entropies of the transition metal doped VO_2 were calculated using both experimental data and DFT calculations. Based on these results, the MIT temperature was associated with lattice distortion of VO_2 (M_1) upon doping, the expansion of cell volume and the decrease in β-angle were associated with the decrease in MIT temperature, and the shrinkage of cell volume and the increase in β-angle the increase in MIT temperature. And it was also concluded that VO_2 (M_1) doped with high valence cations are more stable than those doped with low valence cations. These conclusions are consistent with experimental facts that W-, Mo-, and Re- are the most studied and the most effective dopants for the reducing of MIT temperature, and La-, Hg-, and Ag-doped VO_2 undergoes phase separation.

* Corresponding author. Tel.: 8621-66132405, fax: 8621-66132405. E-mail: liuming.yan@shu.edu.cn.

In addition, DFT calculations without spin-polarization were also carried, and the influences from spin-polarization were evaluated. Finally, scandium was proposed as a potential dopant for VO_2 in view of balanced comprehensive performances.

Keywords: VO_2, thermochromic material, density functional theory, materials design, metal-insulator transition

1. Introduction

Vanadium dioxide (VO_2) has been considered as a typical thermochromic coating material for smart windows to modulate infrared transmission, blocking infrared transmission in summer and allowing infrared transmission in winter from the solar radiation, because of its reversible metal-insulator transition (MIT) between a high-temperature metallic tetragonal rutile phase (R) and a low-temperature semiconducting monoclinic phase (M_1) at critical temperature (T_c) [1]. At transition temperature, VO_2 converts from a reflective state to a transparent state for the near-infrared radiation while remaining almost intact for the visible radiation and thus allowing the modulation of infrared transmission from solar radiation into the building interior by coating VO_2 on window glass [2]. By regulating the critical temperature of the coating material VO_2, best modulation effect, allowing more infrared radiation in winter and blocking more infrared radiation in summer, could be realized [3]. The pristine VO_2 is almost useless as coating material for smart windows as its critical temperature is at 68 ℃, much higher than the comfortable room temperature at about 25 ℃. Besides suitable critical temperature, the commercial value of a potential thermochromic coating material depends on its modulation ratio, the ratio of overall infrared transmission ratio between the summer season and the winter season, and overall visible transmittance. From these aspects, the pristine VO_2, possessing a modulation ratio no larger than 10% and visible transmittance at about 40%, is considered little commercial value as coating

material for smart windows [3]. In addition, the unfavorable brownish color of VO_2 depreciates further its commercial value [4]. Therefore, the modulation of critical temperature and the regulation of transmission spectrum both in the infrared and in the visible range are important for the potential thermochromic coating material based on VO_2.

The modulation of critical temperature and the regulation of transmission spectrum of VO_2 are realized by doping in practice. For example, if a few percent of cations V^{4+} are substituted by high valence transition metal cations W^{6+}, Mo^{6+}, Ta^{5+}, Nb^{5+}, or Ru^{4+}, the critical temperature is effectively modulated [5]. At a doping level of 7 at.% (atomic percent), the critical temperature of Mo-doped VO_2 decreases to 24 ℃ [6], and at a doping level of about 2 at.%, the reversible phase transition of W-doped VO_2 decreases to room temperature [7]. However, Cr^{3+} or Fe^{3+} doping increases the critical temperature by approximately 1 or 3 ℃ per at.% [8, 9]. In addition, the doping of Mg^{2+} could effectively regulate its color because the Mg^{2+} dopant induces a blue-shift to the absorption edge by broadening of the band gap between O-2*p* and V-3*d* t_{2g} [4, 10-12]. Besides the substitution of cation V^{4+} with other cations, the substitution of anion O^{2-} with other anions could also impact the characteristics of VO_2. For example, by substitution of 2.93 at.% of O^{2-} with F^-, not only the critical temperature could be decreased to 35 ℃, but also the O-2*p* band structure could be adjusted resulting in better visible transmission and favorable coloring [13]. However, these experimental studies also revealed the difficulties to simultaneously improve the various properties of VO_2 and thus its comprehensive performances.

Density functional theory (DFT) calculations are important in the understanding of characteristics of pristine and doped VO_2. For example, Yuan et al. explained the ultrafast photo-induced MIT in terms of photo-excited holes, which weakens the V-V interaction and eventually results in the break of V-V dimers, based on DFT calculations [14]. Zhang, Qu, and Pan

et al. suggested that the V-V dimerization plays a more critical role in the transition from the VO_2 (M_1) to the VO_2 (R) compared with the formation of the tetragonal lattice and predicted the transition temperature of W-doped VO_2 in terms of energy difference between these two phases [15, 16]. Despite of the great successes of DFT calculations, it is still difficult to accurately predict the subtle differences between the VO_2 (M_1) and the VO_2 (R) [17]. To our knowledge, there is no known single functional that could simultaneously describe the energy, structure, and electronic and magnetic properties of the VO_2 (M_1) and VO_2 (R) phases. The local density approximation (LDA) and generalized gradient approximation (GGA) functionals could successfully predict the electronic structure of VO_2 (R), but failed to the electronic structure of VO_2 (M_1) because of the strong correlation [18]. The Heyd-Scuseria-Ernzerhof (HSE) functional could correctly predict the VO_2 (R) phase as metallic only in nonmagnetic configuration, but failed in ferromagnetic and antiferromagnetic configuration [19, 20]. The GGA+U method, where U is an effective interaction parameter, could effectively improve the prediction of electronic structures of both VO_2 (R) and VO_2 (M_1), but the calculated total energies are sensitive to the value of U [21]. As a result of compromising, the PBE+U method and HSE functional are used, respectively, to predict the structure and energetics and optical properties of the VO_2 based material. Such compromising practices are fruitful as Wei et al. correctly predicted that both VO_2 (R) and VO_2 (M_1) phases are energetically stabilized by hydrogenation using the GGA+U method [22], and Hu et al. successfully reproduced the blue-shift of absorption edge for the Mg-doped VO_2 using HSE functional [10].

In order to search for an optimized thermochromic coating material being balanced among adequate critical temperature, stability, large modulation ratio, and favorable color, a systematic investigation of the impacts from all the transition metal dopants on the characteristics of VO_2 will be carried out using DFT calculations in this work. The impacts of transition metal dopants on the

MIT critical temperature will be evaluated in terms of lattice distortion of VO_2 (M_1), and the stabilities of transition metal doped VO_2 (M_1) be evaluated in terms of decomposition enthalpies and entropies. These calculations will provide essential information for the search of dopants with optimized comprehensive characteristics of thermochromic coating material based on transition metal doped VO_2.

2. Methodology

2.1 Density functional theory calculations

For the sake of consistency, the energies and structural parameters of the pristine or transition metal doped VO_2, as well as that of the doping elements (the transition elements), were acquired from DFT calculations. Periodic boundary conditions were applied to the calculation cells (super cells) of the pristine or transition metal doped VO_2, corresponding to 1x2x2 primitive cells consisting of sixteen VO_2 units. And the doping ratio was set to 1/16, or one of the V atoms was substituted by one doping atom in each super cell.

The PBE functional [23] with supplement of a Hubbard *U* for the V 3d states [24] was applied to predict the structures and energetics using plane wave basis set and pseudo-potentials as implemented in the VASP program [25-27]. And a Hubbard *U* at 3.5 eV was used for the vanadium atom [16], but not the other transition metal dopants or the Hubbard *U* for the other transition metal dopants was set to zero. The electronic wave functions, with spin-polarization allowed, were expanded using the plane wave base functions with cutoff energy of 600 eV and digitized using the tetrahedron algorithm with Blöchl corrections [28]. The convergent criterion of geometrical optimization was set to 0.01 $eV \cdot Å^{-1}$ for maximum force acted on each atom. The Brillouin-zone

integrations were carried out using the Monkhorst-Pack grids with a 4x4x4 mesh for pristine or transition metal doped VO_2 and with a 8x8x8 mesh for metallic elements [29].

Considering that the PBE+*U* method overestimates the localization effects of *d*-electrons and predicts magnetic ground state even for pristine VO_2 (M_1), inconsistent with experimental observations [30], PBE+*U* calculations without spin-polarization were also carried out for the pristine VO_2 (M_1), as well as for all the transition metal doped VO_2 (M_1), and were shown in **section 3.5**. And the influences of magnetism to the equilibrium lattice parameters, formation energies, and relative stabilities were discussed.

2.2 Bulk modulus and equilibrium properties

The bulk modulus B_0 and equilibrium volume V_0 were evaluated by fitting the DFT calculated free energies to the Birch-Murnaghan equation of states [31, 32],

$$U(V) = U_0 + \frac{B_0 V}{B_0'}\left(\frac{(V_0/V)^{B_0'}}{B_0'-1}+1\right) - \frac{B_0 V_0}{B_0'-1} \quad (1)$$

where $U(V)$ is free energy generated from DFT calculation at 0 K by setting the lattice volume to V, U_0 is the fitted equilibrium free energy and B_0' is the first derivative of bulk modulus with respect to pressure.

2.3 Stability of transition metal doped VO_2

The stability of transition metal doped VO_2 was evaluated from the decomposition reaction,

$$M_xV_{1-x}O_2 \rightarrow (1-x)VO_2 + xMO_y + x(2-y)O_2 \quad (2)$$

And the reaction enthalpy is,

$$\Delta H = (1-x)\Delta_f H[VO_2] + x\Delta_f H[MO_y] + x(2-y)\Delta_f H[O_2] - \Delta_f H[M_xV_{1-x}O_2] \quad (3)$$

where the right side terms are formation enthalpies of VO_2, MO_y (M represents transition metal), O_2, and $M_xV_{1-x}O_2$, respectively. And the formation enthalpies for MO_y and O_2 were adopted from

experimental values as reported in literatures and summarized in **table 1** [33], and the formation enthalpy for $M_xV_{1-x}O_2$ was approximated as the DFT calculated Helmholtz free energy by neglecting of the *pV* term for condensed matter and setting the contribution from entropy to zero at 0 K.

In order to evaluate formation Helmholtz free energy of $M_xV_{1-x}O_2$ from DFT calculations, the following equation was used,

$$(1-x)\,\mathrm{V} + x\,\mathrm{M} + \mathrm{O_2} \rightarrow \mathrm{M}_x\mathrm{V}_{1-x}\mathrm{O_2} \tag{4}$$

And the formation Helmholtz free energy of $V_{1-x}M_xO_2$ at 0 K was evaluated as,

$$\Delta_f U[\mathrm{M}_x\mathrm{V}_{1-x}\mathrm{O_2}] = U[\mathrm{M}_x\mathrm{V}_{1-x}\mathrm{O_2}] - (1-x)U[\mathrm{V}] - xU[\mathrm{M}] - U[\mathrm{O_2}] \tag{5}$$

where the *U*'s in right side are free energies evaluated from DFT calculations of the corresponding components. And the $\Delta_f H[\mathrm{M}_x\mathrm{V}_{1-x}\mathrm{O_2}]$ was approximated as $\Delta_f U[\mathrm{M}_x\mathrm{V}_{1-x}\mathrm{O_2}]$ for condensed matter at 0 K. The Helmholtz free energy for VO_2 was evaluated from the following reaction,

$$\mathrm{V} + \mathrm{O_2} \rightarrow \mathrm{VO_2} \tag{6}$$

And the formation Helmholtz free energy of $V_{1-x}M_xO_2$ at 0 K was evaluated as,

$$\Delta_f U[\mathrm{VO_2}] = U[\mathrm{VO_2}] - U[\mathrm{V}] - U[\mathrm{O_2}] \tag{7}$$

In the DFT+*U* calculations of transition metals, their crystal structures were referred to the stable structures at room temperature [34].

The entropy difference between the transition metal doped VO_2 and pristine VO_2 was evaluated from the Bragg-Williams mixing rule[35],

$$\Delta_{\mathrm{mix}} S = -k_B\left(x\ln x + (1-x)\ln(1-x)\right) \tag{8}$$

where k_B is the Boltzmann constant, x is the molar fraction of the dopant. In addition, the contribution from oxygen vacancies and interstitial oxygen atoms was complemented, and the overall entropy change of decomposition reaction (2) was evaluated as,

$$\Delta S = \Delta_{mix} S - x(2-y)\Delta S[O_2] \quad (9)$$

2.4 Calculation procedure and calculated systems and properties

The calculation procedure was as follows: First, the pristine VO_2 (M_1) (in terms of $V_{16}O_{32}$) and the transition metal doped $MV_{15}O_{32}$ (M = Sc to Zn, Y to Cd, La to Hg, except the radioactive Tc) were partially optimized using DFT + U method at a series of fixed volumes for every systems. Second, the calculated free energies and corresponding volumes for each system were fitted to the Birch-Murnaghan equation of states, and the minimum volume was obtained [31, 32]. Third, another partial optimized was conducted based on the same DFT + U method, and the crystal parameters, free energies, Fermi energies were obtained for all the systems. Fourth, the free energies of 29 transition metals (except the radioactive Tc) and oxygen were obtained using the same DFT + U calculations.

Based on these DFT + U calculations, the formation energies of all the $MV_{15}O_{32}$ were calculated using Eq.(5). The decomposition enthalpies of $MV_{15}O_{32}$ (the decomposition reactions of Eq.(2)) were calculated based on Eq.(3), where the formation energies of MO_y and O_2 were adopted from experimental values as reported in literatures and summarized in **table 1** [33]. The reaction entropies of Eq.(2) were calculated from Bragg-Williams mixing rule based on statistic mechanics.

3. Results and discussion

3.1 Structural optimization and equilibrium energies

We carried out partial structural optimizations of the pristine or transition metal doped VO_2 (M_1) by fixing of the super cell volume at a series of values, and fitted the optimized free energies to the Birch-Murnaghan equation of states as shown in **figure 1**. The curve fittings converge satisfactory except the Fe-, Zn-, Cd-, La-, Os-, Ir-, Pt-doped VO_2 (M_1), for such cases, a B_0' value of 3.5 was applied. And the fitted equilibrium cell volume V_0 and bulk modulus B_0 and its first derivative with to pressure B_0' were summarized in **table 2**. Based on the equilibrium cell volume V_0, a final DFT calculation was carried out and the final lattice parameters a, b, c, and β, free energy U_0, and Fermi energy E_f of the system were obtained as summarized in **table 2**.

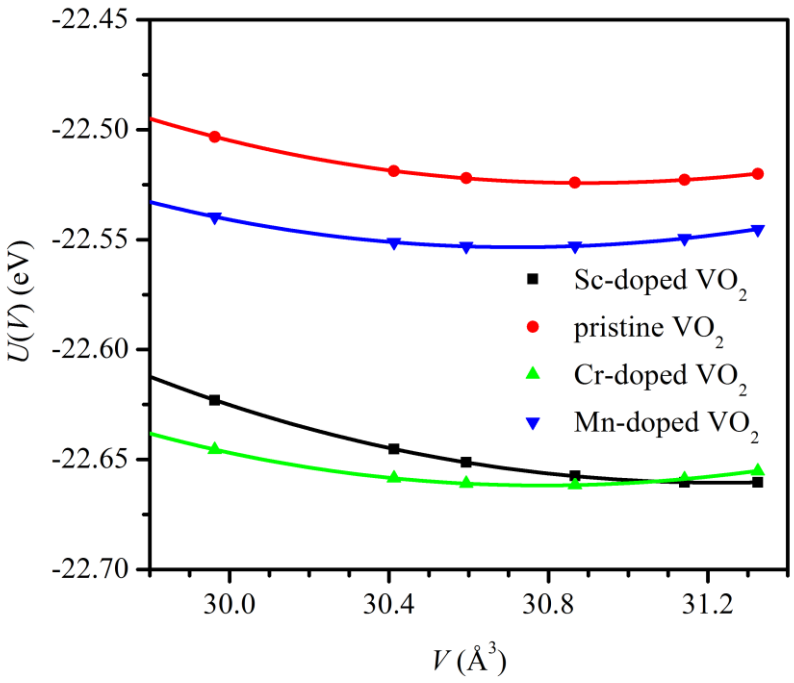

Fig. 1 Examples of the fitting of optimized free energies to the Birch-Murnaghan equation of states for pristine and transition metal doped VO_2

3.2 Prediction of MIT temperature from DFT calculations

3.2.1 Lattice distortion during the MIT

Since the VO_2 (R) and the VO_2 (M_1), belonging to the P42/*mnm* and P21/*c* space groups, respectively, possess different lattice symmetries, a direct comparison of their lattice parameters is impossible. However, these two phases do share the same atomic arrangement with VO_6 octahedrons arranged along their *c*-axes sharing one common edge, and their most significant structural difference is the relative distances between two adjacent V atoms: the V-V distances in VO_2 (R) are equivalent but that in VO_2 (M_1) are inequivalent varying alternatively. In order to compare their structural differences between VO_2 (M_1) and VO_2 (R), we identified corresponding lattice parameters a', b', c' and β' in VO_2 (R) corresponding to the lattice parameters a, b, c and β in VO_2 (M_1) as shown in **figure 2**. And we will focus on the changes in these corresponding lattice parameters during MIT in the following context.

From the corresponding lattice parameters as shown in **figure 2** and **table 3** [36], it is noticed that the lattice parameters a and b slightly expand from 5.375 Å and 4.526 Å for VO_2 (M_1), respectively, to 5.383 Å and 4.554 Å for VO_2 (R) during the MIT. While the lattice parameter c shrinks from 5.753 Å to 5.712 Å, and the β angle decreases from 122.6 ° to 122.1 °. Comprehensively, the cell volume expands from 118.07 $Å^3$ to 118.44 $Å^3$ during the MIT. Though the changes in corresponding lattice parameters between VO_2 (M_1) and VO_2 (R) are small, these changes do cause great changes in their band structures and optical properties [1, 2, 37].

Based on these observations, we propose that if a dopant causes changes in corresponding lattice parameters of VO_2 (M_1) resembling to those of VO_2 (R), the dopant will lower the MIT temperature. Therefore, the changes in corresponding lattice parameters between the pristine and the transition metal doped VO_2 may be used as criteria to screen out any transition metal dopants that lower the MIT temperature and to cause large changes in band structures and optical properties.

We noticed an interesting comment about the structure and the β-angle in literatures [5, 30]. The remaining one *d*-electron in VO_2 (M_1) occupies in the $d_{x^2-y^2}$ orbit along the *c* -axis, whereas the *d*-electron in VO_2 (*R*) is itinerant among the d_{yz}, d_{zx} and $d_{x^2-y^2}$ orbits. Since the d_{yz} and d_{zx} orbits are perpendicular to the *c*-axis, the β-angle reflects, to some extent, the ratio of electrons in d_{yz} and d_{zx} and in $d_{x^2-y^2}$. That is to say, if more *d*-electron occupied d_{yz} and d_{zx} orbits, the β-angle will reduce and the structure of doped VO_2 (M_1) will close to VO_2 (*R*). In fact, the tetragonal-like structure of W-doped VO_2 (M_1) (the W is the most studied dopant that reduces the MIT temperature) has been reported by X-ray absorption spectroscopy coupled with first principle calculations [38].

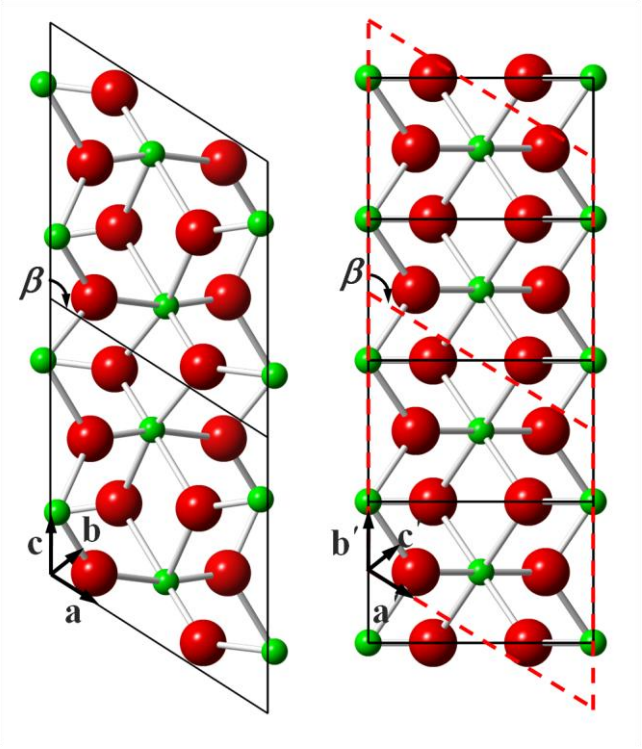

Fig. 2 Definition of corresponding lattice parameters between VO_2 (M_1) (left) and VO_2 (*R*) (right), and their experimental values (see **table 3**).

3.2.2 Relationship between MIT and corresponding lattice parameters

As the temperature increases to T_c, a low-temperature semiconducting monoclinic VO_2 (M_1) phase converts into a metallic phase with symmetrical structure of VO_2 (R). Meanwhile, the corresponding lattice parameters undergo slight changes, and the expansion of corresponding lattice volume and the decreasing of β angle induced by electron redistribution are related to the decrease in MIT temperature.

The corresponding lattice parameters evaluated from DFT calculations with spin-polarization for transition metal doped VO_2 (M_1) were summarized in **table 2**. And the distribution diagram, which shows the distribution of transition metal doped VO_2 (M_1) on the V_0~β plane, where V_0 and β are DFT calculated volume and β-angle of the optimized super cell in terms of $M_{0.0625}V_{0.9375}O_2$ (M_1) in this work, is used to show the structural distortion and similarity of VO_2 (M_1) upon doping. The distribution diagram shows not only the structural distortion of $M_{0.0625}V_{0.9375}O_2$ (M_1), the greater the distortion, the further the scattering data point from the pristine VO_2 (M_1) on the V_0~β plane, but also the structural similarity of VO_2 (M_1) doped with various transition metals, the more the similarity in structures, the closer the scattering data points on the V_0~β plane. From **figure 3**, it could be seen that the W-, Mo-, or Re-doped VO_2 (M_1) were distributed at the bottom right corner of the V_0~β plane, greatest increase in V_0 and decrease in β. These are the most effective doping elements to reduce the critical temperature as reported in experiments [5, 39]. By contrast, Fe-doping results in greatest volume shrinkage as predicted by our DFT calculations, and the Fe-doping causes the increase in MIT temperature reported in experiment [5, 9]. In addition, Pan et al. suggested that Cr-doping will result in shrinkage of lattice volume, Brown, et al. observed the increase in transition temperature in Cr-doped VO_2 [8, 40]. These facts are consistent with our

calculation results as shown in **figure 3**. From the distribution diagram, it could be seen that most of the fourth series transition metals caused the volume shrinkage if they are doped to VO_2 (M_1). On the other hand, the doping of Ru, Rh, Pd, Os, and Ir will cause the expansion of VO_2 (M_1), thus significantly decrease in MIT temperature. From **table 4** where the most studied dopants and their influences to the transition temperature are summarized, it could be concluded that our calculations summarized in **figure 3** are consistent with experimental observations.

From these observations, it is proposed that the scandium, which causes the expansion of volume and the decrease in β-angle and is in adjacent to the elements that most effectively causes the decrease in MIT temperature in **figure 3**, would be a potential dopant that decreases the MIT temperature. In addition, the trivalent cation Sc^{3+} possesses no *d*-electron and the electrostatic attraction between the trivalent cation Sc^{3+} and anion O^{2-} is weaker than that between the tetravalent cation V^{4+} and anion O^{2-}, and thus Sc^{3+} might induce a blue-shift to the absorption edge resembling to Mg^{2+} or F^- [4, 10-13]. The other elements that cause greatest decrease in β-angle include Cu, Zn, and Co, and cause greatest expansion in volume include La, Y, Hg, Zr, Pt, and Hf.

In order to evaluate the influences of V-V dimerization to the MIT temperature, the V-V distance changes and V-V dimer distortion angles in the pristine and transition metal doped M-VO_2 (M_1) were summarized in **table 5**. In overall, the changes between the long and the short V-V distances are small, only two dopants, Co and Cu, cause the V-V distance changes greater than 0.1 Å, six dopants, W, Re, Mo, Sc, La, and Nb, cause the V-V distance changes greater than 0.01 Å and less than 0.1 Å, and the other dopants cause the V-V distance changes less than 0.01 Å, with a maximum value of 0.069 Å and an average value of 0.018 Å. For the pristine VO_2 (M_1), the short and long V-V distances are at 3.0385 and 3.0390 Å, with negligible change. It is difficult to explain why the dopants Co and Cu cause such large V-V distance changes, since the Cu only

causes moderate MIT temperature decrease [41] and Co has not been reported to be effective dopant. However, the dopants W, Re, Mo, and Nb are among the most effective dopants ever studied as summarized in **table 4**. Therefore, it is reasonable to propose that Sc and La might be potential dopants to decrease the MIT temperature of VO_2.

For the V-V dimer distortion angle, the La dopant causes the greatest distortion angle at 162.5 °, and Sc, Y, Cd, and Hg causes the distortion angle less than 175 °, and Mo and W cause the distortion angle at 176.3 ° and 178.3 °, respectively. These results are not enough to deduce decisive conclusions.

In summary, decisive conclusions cannot be deduced that the calculated V-V distance changes and V-V dimer distortion angles can be related to the MIT temperature of the transition metal doped VO_2, however, these results do provide a hint that a dopant causes V-V distance change will cause MIT temperature decrease, and Sc and possibly La might be potential dopants for the modulation of MIT temperature of VO_2 (M_1).

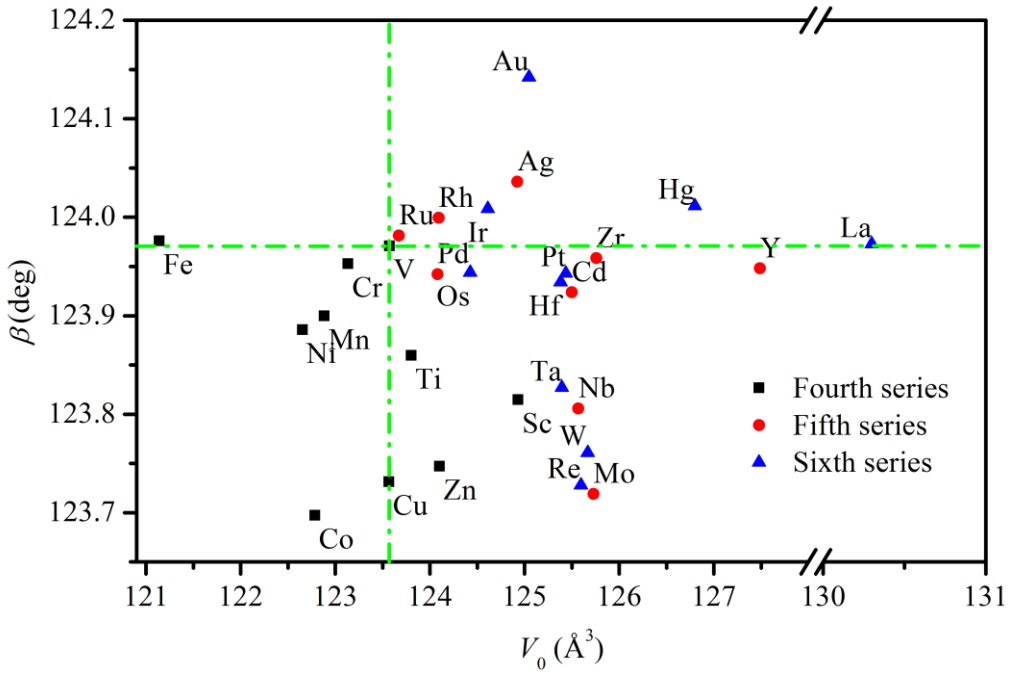

Fig. 3 Distribution diagram of the transition metal doped VO_2 (M_1), labeled by the dopant metal only, on the V_0~β plane, where V_0 and β are calculated volume and β-angle of the optimized super cell in terms of $M_{0.0625}V_{0.9375}O_2$ (M_1) with spin-polarization. The green dash-dot lines represent the volume and β-angle of the pristine VO_2 (M_1) calculated at the same level of theory

3.3 Formation enthalpies for transition metal doped VO_2 (M_1)

The free energies for the transition metal doped VO_2 (M_1), in terms of $M_{0.0625}V_{0.9375}O_2$ (M_1), were summarized in **table 2** and shown in **figure 4a**. From **figure 4a**, it could be seen that the free energies firstly decrease with the group number of dopants in the periodic table of elements and reach a minimum value at the VB-group, and then increase with the group number. However, abnormal changes were observed for the IIB-group. When going from the top to the bottom of every group in the periodic table of elements, the free energies generally decrease for the IVB-group to the VIII-group, while increase for the IIIB-, IB-, and IIB-groups in the head or tail of the series of elements. As a result, the Ta-doped VO_2 (M_1) possesses the lowest while Hg-doped the highest free energies among all transition metal doped VO_2 (M_1).

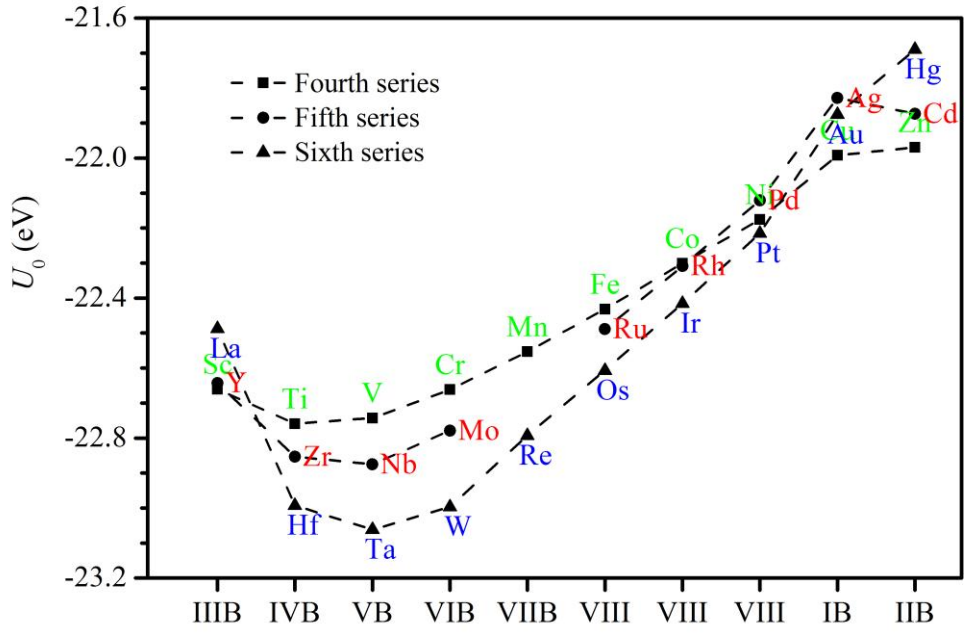

(a)

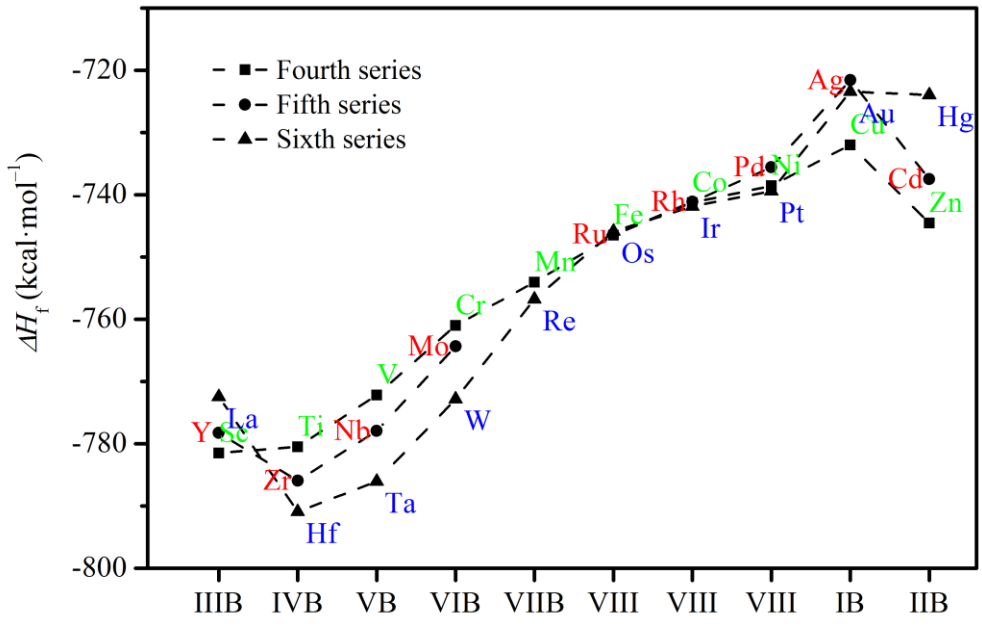

(b)

Fig. 4 The free energies (a) and formation enthalpies (b) of transition metal doped VO_2 (M_1). Notice that the free energy for pristine VO_2 (M_1) is compensated by the Hubbard-*U* term as used in

the DFT calculation and the DFT calculations are carried out with spin-polarization (the dash lines are only guide to the eyes)

The formation enthalpies for the transition metal doped VO_2 (M_1) are also summarized in **table 1**. The calculated formation enthalpy of VO_2 was -772.2 kJ mol^{-1} at 0 K, comparable to experimental value of -717.6 kJ/mol at 298.15 K [42]. Except for the IIIB and IIB dopants, the formation enthalpies for the $M_{0.0625}V_{0.9375}O_2$ (M_1) increase monotonically as the dopant goes from left to right in the periodic table of elements (**figure 4b**).

The free energies and formation enthalpies calculated without spin-polarization will be reported in **section 3.5**.

3.4 Stability of transition metal doped VO_2

The stability of a transition metal doped VO_2 could be evaluated in terms of Gibbs free energy of its decomposition reaction. Considering that the Gibbs free energy of the decomposition reaction (2) could be evaluated as,

$$\Delta G = \Delta H - T\Delta S \tag{10}$$

therefore, it is possible to evaluate the stability in terms of decomposition enthalpy and entropy.

In **figure 5**, it shows the distribution diagram of transition metal doped VO_2 (M_1) at doping ratio of 1/16 on the ΔH~ΔS plane. The decomposition entropy consists of the mixing entropy and the contributions from oxygen vacancies and interstitial oxygen as shown in equation 9. The VO_2 (M_1) doped with high valence cation possesses negative decomposition entropy and the decomposition reaction is unfavorable, or the VO_2 (M_1) doped with high valence cation is more stable than that doped with low valence cation. In addition, a positive change in decomposition enthalpy represents that the transition metal doped VO_2 (M_1) is stable. Such prediction of stability

of transition metal doped VO_2 (M_1) is consistent with experimental observations. For example, experimental observation showed that the Zn-, Y-, and La-doped VO_2 exhibit phase separation phenomenon and is thus unstable, in our calculations as shown in **figure 5**, these metal doped VO_2 are among the most unstable systems [43]. On the other hand, the W-, Re-, Os-, Ta-doped VO_2 are among the most stable systems in experimental observations, and are also the most stable systems from our calculation prediction [5]. From these considerations, it could be concluded that the Ru-doped VO_2 is the most stable system among all the transition metal doped VO_2 (**figure 5**).

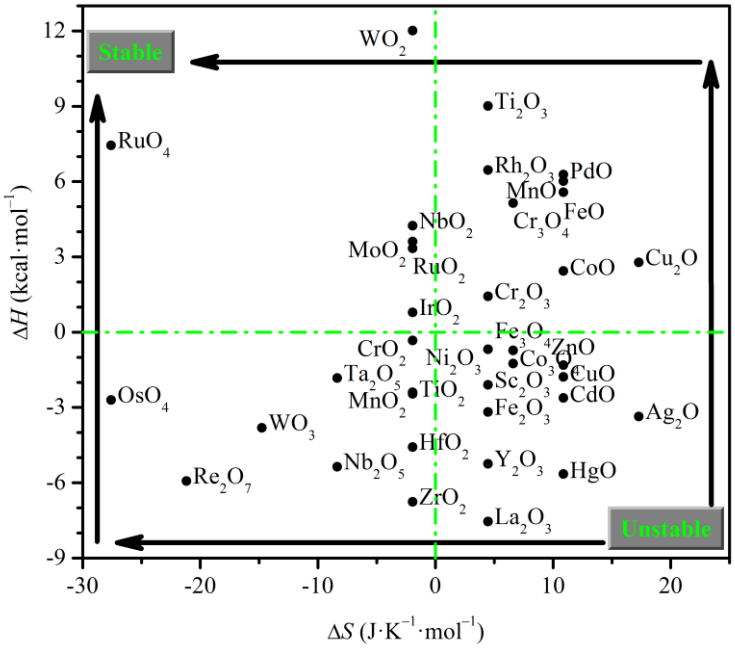

Fig. 5 Decomposition enthalpies and entropies for the transition metal doped VO_2 (M_1) calculated using eq. 3 and eq. 9, the DFT calculations are with spin-polarization

From the structural distortion, we proposed that the Sc is a potential dopant for the modulation of MIT temperature of VO_2. Though the Sc does not belong to the group of dopants forming most stable VO_2, the Sc-doped VO_2 is in the middle of **figure 5** and thus is predicted to be

stable enough for practical application. Compared to Mg-doped VO_2, Sc has a larger diameter and higher valence than Mg, therefore, the Sc-doped VO_2 may be more stable than the Mg-doped VO_2.

3.5 Influences of spin-polarization to calculation results

The detailed calculation results without spin-polarization were summarized as supplementary information as **tables SI-1 and SI-2**. It is interesting that the formation enthalpy for VO_2 (M_1) calculated without spin-polarization is -713.6 kJ·mol^{-1}, which is very close to the experimental value of 717.6 kJ·mol^{-1} as show in **table 1**. In overall, the free energies calculated with spin-polarization (**table 2**) are lower than those calculated without spin-polarization (**table SI-2**). From the free energy differences calculated without spin-polarization to with spin-polarization as shown **figure 6**, it could be seen that the free energy differences vary from 0.481 eV to 0.635 eV with an average value of 0.569 eV. These values are significant in absolute, however, they are relatively unimportant if we regard these values as systematic errors and thus only the differences between the individual errors and the average error matter. Compared to the free energy differences which span a range of only 0.154 eV, the free energies which vary from -23.062 eV to -21.690 eV, span a range of 1.372 eV. Therefore, it could be concluded that overall conclusions, which relate to the free energies and properties deduced (enthalpies and stabilities), deduced from DFT calculations with spin-polarization will not be significantly affected if the spin-polarization was turned off.

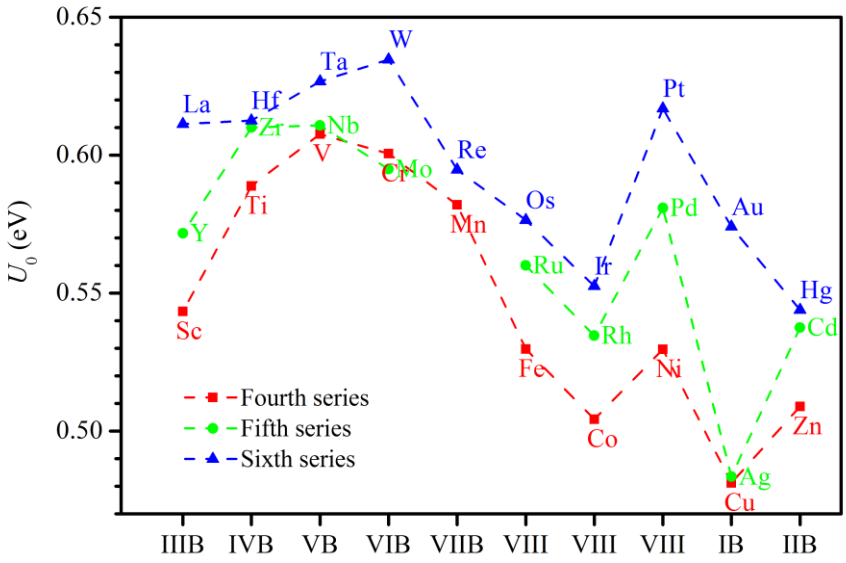

Fig. 6 The free energies differences calculated without spin-polarization to with spin-polarization, and the free energies are scaled to one $M_{0.0625}V_{0.9375}O_2$ (M_1) unit

From the comparison of cell volumes calculated with or without spin-polarization (**figure 7a**), it could be seen that moderate linear relationship between these two sets of cell volumes exists (the correlation coefficient is 0.779). Again, it could be concluded that the overall conclusions, which relate to cell volume change, deduced from DFT calculations with spin-polarization will not be significantly affected if the spin-polarization was turned off.

For **figure 7b**, it could be seen that the β-angles calculated with spin-polarization vary irregularly with those calculated without spin-polarization, and there is no obvious relationship between these two sets of data. Therefore, the conclusions, which relate to the β-angles, deduced from DFT calculations with spin-polarization might be affected if the spin-polarization was turned off.

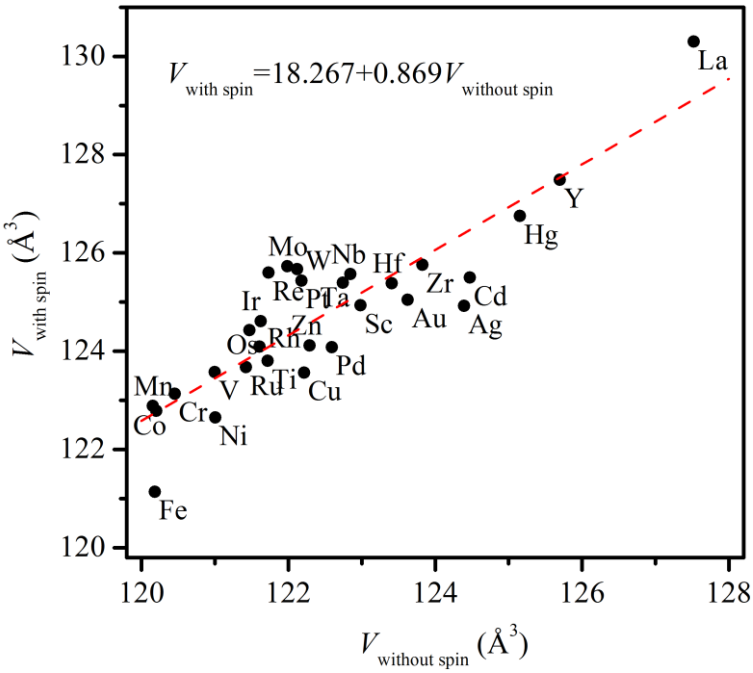

(a)

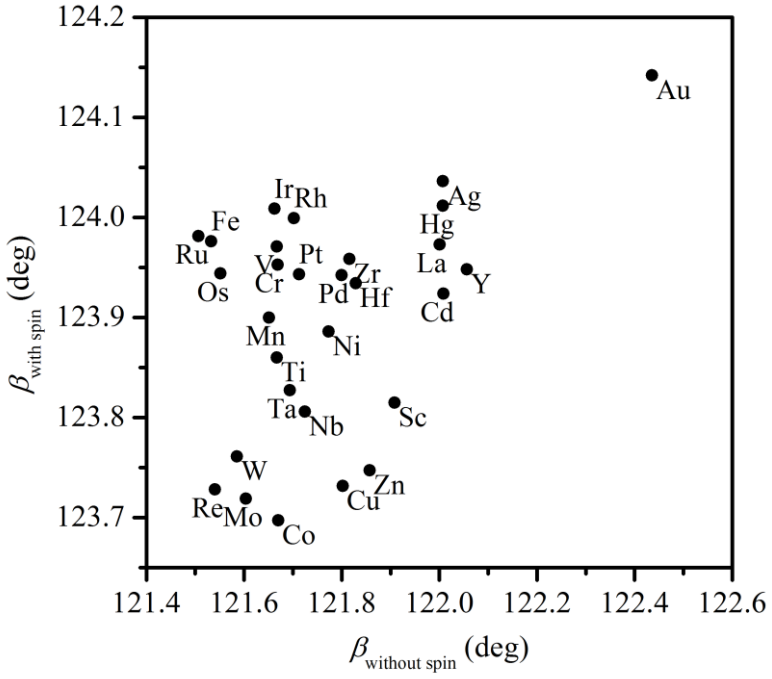

(b)

Fig. 7 Comparison of (a) cell volumes and (b) β-angles for the transition metal doped VO_2 (M_1) calculated with and without spin-polarization

In overall, it could be concluded that calculation differences with/without spin-polarization do exist and cannot be ignored, however, the overall conclusions summarized in this study relied only on the relative values between the pristine and transition metal doped VO_2 (M_1). And the calculation differences of relative values with/without spin-polarization cancel each other, and the overall conclusions deduced in this work will not be affected significantly if these conclusions are not used for the prediction of individual M-doped VO_2 (M_1).

4. Conclusions

Density functional theory calculations based on the PBE+U method were carried out for all the transition metal doped VO_2 (M_1). The MIT temperature was associated with the lattice distortion, or changes in volume and β-angle of the transition metal doped VO_2 (M_1). The more the lattice expansion and β-angle decrease, the lower the transition temperature of the transition metal doped VO_2 (M_1) will be, and the more the lattice shrinkage and β-angle increase the higher the transition temperature of the transition metal doped VO_2 (M_1).

The decomposition enthalpies of the transition metal doped VO_2 (M_1) were calculated based on experimental enthalpies of doping oxides and free energies of the doped VO_2 (M_1) from DFT calculations. And the entropies were evaluated by use of the Bragg-Williams mixing rule and entropies of oxygen vacancies and interstitial oxygen atoms. Based on these enthalpies and entropies, the stabilities of the transition metal doped VO_2 (M_1) were evaluated and it was concluded that the VO_2 (M_1) doped with high valence cations are more stable than those doped with low valence cations. Especially, the Ru- and W-doped VO_2 (M_1) were the most stable ones and the La-, Ag- and Hg-doped VO_2 (M_1) were least stable ones and would undergo phase

separation. These conclusions are important for the selection of transition metal dopants in the design and preparation of transition metal doped VO_2 (M_1).

Considering the influences from spin-polarization, DFT calculations without spin-polarization were also carried. It was concluded that calculated free energies with spin-polarization are lower than those without spin-polarization, however, the relative differences among various doped systems are insignificant. In addition, there is moderate linear relationship between cell volumes calculated with and without spin-polarization. Therefore, the overall conclusions deduced from calculations with spin-polarization will not be affected if these conclusions are not used for the prediction of individual M-doped VO_2 (M_1).

Finally, Sc was proposed to be a potential dopant to modulate the MIT temperature and to improve the optical spectrum. In addition, the Sc-doped VO_2 (M_1) was predicted to be stable enough for practical application.

Acknowledgements

The authors thank the financial support from the Chinese National Science Foundation (Nos. 21073118, 21376147), the Innovation Program of Shanghai Municipal Education Commission (13ZZ078), and the 085 Knowledge Innovation Program, and they acknowledge the High Performance Computing Center and Laboratory for Microstructures, Shanghai University, for computing and structural characterization support.

References

[1] F. Morin, Oxides Which Show a Metal-to-Insulator Transition at the Neel Temperature. Phys. Rev. Lett. **1959**, 3(1): 34-36.

[2] T. D. Manning, I. P. Parkin, M. E. Pemble, D. Sheel, and D. Vernardou, Intelligent Window Coatings: Atmospheric Pressure Chemical Vapor Deposition of Tungsten-Doped Vanadium Dioxide. Chem. Mater. **2004**, 16(4): 744-749.

[3] S. Y. Li, G. A. Niklasson, and C. G. Granqvist, Thermochromic Fenestration with VO_2-Based Materials: Three Challenges and How They Can Be Met. Thin Solid Films **2012**, 520(10): 3823-3828.

[4] J. D. Zhou, Y. F. Gao, X. L. Liu, Z. Chen, L. Dai, C. X. Cao, H. J. Luo, M. Kanahira, C. Sun, and L. M. Yan, Mg-Doped VO_2 Nanoparticles: Hydrothermal Synthesis, Enhanced Visible Transmittance and Decreased Metal-Insulator Transition Temperature. Phys. Chem. Chem. Phys. **2013**, 15(20): 7505-7511.

[5] J. B. Goodenough, The Two Components of the Crystallographic Transition in VO_2. J. Solid State Chem. **1971**, 3(4): 490-500.

[6] T. J. Hanlon, J. A. Coath, and M. A. Richardson, Molybdenum-Doped Vanadium Dioxide Coatings on Glass Produced by the Aqueous Sol-Gel Method. Thin Solid Films **2003**, 436(2): 269-272.

[7] W. Burkhardt, T. Christmann, B. K. Meyer, W. Niessner, D. Schalch, and A. Scharmann, W- and F-Doped VO_2 Films Studied by Photoelectron Spectrometry. Thin Solid Films **1999**, 345(2): 229-235.

[8] B. L. Brown, M. Lee, P. G. Clem, C. D. Nordquist, T. S. Jordan, S. L. Wolfley, D. Leonhardt, C. Edney, and J. A. Custer, Electrical and Optical Characterization of the Metal-Insulator Transition Temperature in Cr-Doped VO_2 Thin Films. J. Appl. Phys. **2013**, 113(17): 173704.

[9] W. Brückner, U. Gerlach, W. Moldenhauer, H. P. Brückner, B. Thuss, H. Oppermann, E. Wolf, and I. Storbeck, Metal-Nonmetal Transition in Fe- and Al-Doped VO_2. J. Phys. Colloques **1976**, 37(C4): 63-68.

[10] S. L. Hu, S. Y. Li, R. Ahuja, C. G. Granqvist, K. Hermansson, G. A. Niklasson, and R. H. Scheicher, Optical Properties of Mg-Doped VO_2: Absorption Measurements and Hybrid Functional Calculations. Appl. Phys. Lett. **2012**, 101(20): 201902.

[11] N. R. Mlyuka, G. A. Niklasson, and C. G. Granqvist, Mg Doping of Thermochromic VO_2 Films Enhances the Optical Transmittance and Decreases the Metal-Insulator Transition Temperature. Appl. Phys. Lett. **2009**, 95(17): 171909.

[12] S. Y. Li, N. R. Mlyuka, D. Primetzhofer, A. Hallen, G. Possnert, G. A. Niklasson, and C. G. Granqvist, Bandgap Widening in Thermochromic Mg-Doped VO_2 Thin Films: Quantitative Data Based on Optical Absorption. Appl. Phys. Lett. **2013**, 103(16): 161907.

[13] L. Dai, S. Chen, J. J. Liu, Y. F. Gao, J. D. Zhou, Z. Chen, C. X. Cao, H. J. Luo, and M. Kanehira, F-Doped VO_2 Nanoparticles for Thermochromic Energy-Saving Foils with Modified Color and Enhanced Solar-Heat Shielding Ability. Phys. Chem. Chem. Phys. **2013**, 15(28): 11723-11729.

[14] X. Yuan, W. Q. Zhang, and P. H. Zhang, Hole-Lattice Coupling and Photoinduced Insulator-Metal Transition in VO_2. Phys. Rev. B **2013**, 88(3): 035119.

[15] J. J. Zhang, H. Y. He, Y. Xie, and B. C. Pan, Theoretical Study on the Tungsten-Induced Reduction of Transition Temperature and the Degradation of Optical Properties for VO_2. J. Chem. Phys. **2013**, 138(11): 114705.

[16] B. Y. Qu, H. Y. He, and B. C. Pan, The Dynamical Process of the Phase Transition from VO_2 (M_1) to VO_2 (R). J. Appl. Phys. **2011**, 110(11): 113517.

[17] Z. Y. Zhu and U. Schwingenschlogl, Comprehensive Picture of VO_2 from Band Theory. Phys. Rev. B **2012**, 86(7): 075149.

[18] R. M. Wentzcovitch, W. W. Schulz, and P. B. Allen, VO_2: Peierls or Mott-Hubbard? A View from Band Theory. Phys. Rev. Lett. **1994**, 72(21): 3389-3392.

[19] R. Grau-Crespo, H. Wang, and U. Schwingenschlögl, Why the Heyd-Scuseria-Ernzerhof Hybrid Functional Description of VO_2 Phases is Not Correct. Phys. Rev. B **2012**, 86(8): 081101.

[20] V. Eyert, VO_2: A Novel View from Band Theory. Phys. Rev. Lett. **2011**, 107(1): 016401.

[21] L. Wang, T. Maxisch, and G. Ceder, Oxidation Energies of Transition Metal Oxides Within the GGA+*U* Framework. Phys. Rev. B **2006**, 73(19): 195107.

[22] J. Wei, H. Ji, W. H. Guo, A. H. Nevidomskyy, and D. Natelson, Hydrogen Stabilization of Metallic Vanadium Dioxide in Single-Crystal Nanobeams. Nat. Nanotechnol. **2012**, 7(6): 357-362.

[23] J. P. Perdew, K. Burke, and M. Ernzerhof, Generalized Gradient Approximation Made Simple. Phys. Rev. Lett. **1996**, 77(18): 3865-3868.

[24] V. I. Anisimov, J. Zaanen, and O. K. Andersen, Band Theory and Mott Insulators: Hubbard *U* Instead of Stoner *I*. Phys. Rev. B **1991**, 44(3): 943-954.

[25] G. Kresse and J. Furthmüller, Efficiency of Ab-Initio Total Energy Calculations for Metals and Semiconductors Using a Plane-Wave Basis Set. Comput. Mater. Sci. **1996**, 6(1): 15-50.

[26] G. Kresse and J. Furthmüller, Efficient Iterative Schemes for Ab Initio Total-Energy Calculations Using a Plane-Wave Basis Set. Phys. Rev. B **1996**, 54(16): 11169-11186.

[27] G. Kresse and D. Joubert, From Ultrasoft Pseudopotentials to the Projector Augmented-Wave Method. Phys. Rev. B **1999**, 59(3): 1758-1775.

[28] P. E. Blöchl, Projector Augmented-Wave Method. Phys. Rev. B **1994**, 50(24): 17953-17979.

[29] H. J. Monkhorst and J. D. Pack, Special Points for Brillouin-Zone Integrations. Phys. Rev. B **1976**, 13(12): 5188-5192.

[30] X. Yuan, Y. B. Zhang, T. A. Abtew, P. H. Zhang, and W. Q. Zhang, VO_2: Orbital Competition, Magnetism, and Phase Stability. Phys. Rev. B **2012**, 86(23): 235103.

[31] F. D. Murnaghan, The Compressibility of Media under Extreme Pressures. Proc. Nat. Acad. Sci. U.S.A. **1944**, 30(9): 244-247.

[32] F. Birch, Finite Elastic Strain of Cubic Crystals. Phys. Rev. **1947**, 71(11): 809-824.

[33] D. R. Lide (ed.), *CRC Handbook of Chemistry and Physics*. Internet Version, **2005**.

[34] G. Zhou and L. Duan, *Introduction to Structure Chemistry*. 5th ed, **2008**. Beijing: Peking University Press.

[35] W. L. Bragg and E. J. Williams, The Effect of Thermal Agitation on Atomic Arrangement in Alloys. Proc. R. Soc. London, Ser. A **1934**, 145(855): 699-730.

[36] K. D. Rogers, An X-Ray Diffraction Study of Semiconductor and Metallic Vanadium Dioxide. Powder Diffr. **1993**, 8(4): 240-244.

[37] M. H. Lee, Thermochromic Glazing of Windows with Better Luminous Solar Transmittance. Sol. Energy Mater. Sol. Cells **2002**, 71(4): 537-540.

[38] X. G. Tan, T. Yao, R. Long, Z. H. Sun, Y. J. Feng, H. Cheng, X. Yuan, W. Q. Zhang, Q. H. Liu, C. Z. Wu, et al., Unraveling Metal-Insulator Transition Mechanism of VO_2 Triggered by Tungsten Doping. Scientific Reports **2012**, 2: 466.

[39] E. E. Chain, Optical Properties of Vanadium Dioxide and Vanadium Pentoxide Thin Films. Appl. Opt. **1991**, 30(19): 2782-2787.

[40] M. Pan, H. M. Zhong, S. W. Wang, Z. F. Li, X. S. Chen, and W. Lu, First-Principle Study on the Chromium Doping Effect on the Crystal Structure of Metallic VO_2. Chem. Phys. Lett. **2004**, 398(4-6): 304-307.

[41] S. W. Lu, L. S. Hou, and F. X. Gan, Synthesis and Phase Transition of Cu^{2+} Ion Doped VO_2 Thin Films. J. Mater. Sci. Lett. **1996**, 15(10): 856-857.

[42] J. Qi, G. Ning, and Y. Lin, Synthesis, Characterization, and Thermodynamic Parameters of Vanadium Dioxide. Mater. Res. Bull. **2008**, 43(8-9): 2300-2307.

[43] J. Du, Y. F. Gao, Z. Chen, L. T. Kang, Z. T. Zhang, and H. J. Luo, Enhancing Thermochromic Performance of VO_2 Films via Increased Microroughness by Phase Separation. Sol. Energy Mater. Sol. Cells **2013**, 110: 1-7.

[44] S. Chen, L. Dai, J. Liu, Y. F. Gao, X. Liu, Z. Chen, J. Zhou, C. Cao, P. Han, H. Luo, et al., The Visible Transmittance and Solar Modulation Ability of VO_2 Flexible Foils Simultaneously Improved by Ti Doping: An Optimization and First Principle Study. Phys. Chem. Chem. Phys. **2013**, 15(40): 17537-17543.

[45] J. Du, Y. F. Gao, H. J. Luo, Z. T. Zhang, L. T. Kang, and Z. Chen, Formation and Metal-to-Insulator Transition Properties of VO_2-ZrV_2O_7 Composite Films by Polymer-Assisted Deposition. Sol. Energy Mater. Sol. Cells **2011**, 95(7): 1604-1609.

[46] C. Piccirillo, R. Binions, and I. P. Parkin, Nb-Doped VO_2 Thin Films Prepared by Aerosol-Assisted Chemical Vapour Deposition. Eur. J. Inorg. Chem. **2007**(25): 4050-4055.

[47] L. Q. Mai, B. Hu, T. Hu, W. Chen, and E. D. Gu, Electrical Property of Mo-Doped VO_2 Nanowire Array Film by Melting-Quenching Sol-Gel Method. J. Phys. Chem. B **2006**, 110(39): 19083-19086.

[48] Z. P. Wu, A. Miyashita, S. Yamamoto, H. Abe, I. Nashiyama, K. Narumi, and H. Naramoto, Molybdenum Substitutional Doping and Its Effects on Phase Transition Properties in Single Crystalline Vanadium Dioxide Thin Film. J. Appl. Phys. **1999**, 86(9): 5311-5313.

[49] Y. F. Gao, C. X. Cao, L. Dai, H. J. Luo, M. Kanehira, Y. Ding, and Z. L. Wang, Phase and Shape Controlled VO_2 Nanostructures by Antimony Doping. Energy Environ. Sci. **2012**, 5(9): 8708-8715.

[50] J. Li, D. Dan, N. Yuan, and T. Xie. *Phase Transition Characteristics of Tungsten and Tantalum Doped VO_2 Polycrystalline Thin Films Formed by Ion Beam Enhanced Deposition*. in *3rd International Symposium on Advanced Optical Manufacturing and Testing Technologies: Optical Test and Measurement Technology and Equipment*. **2007**. International Society for Optics and Photonics.

[51] L. T. Kang, Y. F. Gao, H. J. Luo, J. Wang, B. L. Zhu, Z. T. Zhang, J. Du, M. Kanehira, and Y. Z. Zhang, Thermochromic Properties and Low Emissivity of ZnO:Al/VO_2 Double-Layered Films with a Lowered Phase Transition Temperature. Sol. Energy Mater. Sol. Cells **2011**, 95(12): 3189-3194.

Figure Captions

Fig. 1 Examples of the fitting of optimized free energies to the Birch-Murnaghan equation of states for pristine and transition metal doped VO_2

Fig. 2 Definition of corresponding lattice parameters between VO_2 (M_1) (left) and VO_2 (R) (right), and their experimental values (see **table 3**)

Fig. 3 Distribution diagram of the transition metal doped VO_2 (M_1), labeled by the dopant metal only, on the V_0~β plane, where V_0 and β are calculated volume and β-angle of the optimized super cell in terms of $M_{0.0625}V_{0.9375}O_2$ (M_1) with spin-polarization. The green dash-dot lines represent the volume and β-angle of the pristine VO_2 (M_1) calculated at the same level of theory

Fig. 4 The free energies (a) and formation enthalpies (b) of transition metal doped VO_2 (M_1). Notice that the free energy for pristine VO_2 (M_1) is compensated by the Hubbard-U term as used in the DFT calculation and the DFT calculations are carried out with spin-polarization (the dash lines are only guide to the eyes)

Fig. 5 Decomposition enthalpies and entropies for the transition metal doped VO_2 (M_1) calculated using eq. 3 and eq. 9, the DFT calculations are with spin-polarization

Fig. 6 The free energies differences calculated without spin-polarization to with spin-polarization, and the energies are scaled to one $M_{0.0625}V_{0.9375}O_2$ (M_1) unit

Fig. 7 Comparison of (a) cell volumes and (b) β-angles for the transition metal doped VO_2 (M_1) calculated with and without spin-polarization

Table 1. Thermal dynamic properties of the transition metal oxides and $M_{0.0625}V_{0.9375}O_2$ (the DFT calculation are carried out with spin-polarization, units: kJ mol^{-1} for enthalpy and J K^{-1} mol^{-1} for entropy)

Oxides	$\Delta_f H$ [oxide] [(a)]	$\Delta_f H$ [$M_{0.0625}V_{0.9375}O_2$] [(b)]	ΔH [(c)]	ΔS [(d)]
Sc_2O_3	-1908.8	-781.5	-2.10	4.47
TiO	-519.7	-780.5	24.06	10.88
Ti_2O_3	-1520.9	-780.5	9.01	4.47
TiO_2	-944.0	-780.5	-2.46	-1.94
VO_2	-717.6 [(e)]	-772.2	0.0	0.0
Cr_2O_3	-1139.7	-761.0	1.43	4.47
Cr_3O_4	-1531.0	-761.0	5.15	6.60
CrO_2	-598.0	-761.0	-0.33	-1.94
MnO	-385.2	-754.03	6.02	10.88
MnO_2	-520.0	-754.03	-2.40	-1.94
FeO	-272.0	-746.5	5.57	10.88
Fe_3O_4	-1118.4	-746.5	-0.73	6.60
Fe_2O_3	-824.2	-746.5	-3.18	4.47
CoO	-237.9	-741.2	2.44	10.88
Co_3O_4	-891.0	-741.2	-1.25	6.60
Ni_2O_3	-489.5	-738.5	-0.69	4.47
Cu_2O	-168.6	-732.0	2.78	17.29
CuO	-157.3	-732.0	-1.79	10.88
ZnO	-350.5	-744.5	-1.32	10.88

Y_2O_3	-1905.3	-778.2	-5.24	4.47
ZrO_2	-1100.1	-785.9	-6.76	-1.94
NbO	-405.8	-777.9	28.64	10.88
NbO_2	-796.2	-777.9	4.24	-1.94
Nb_2O_5	-1899.5	-777.9	-5.36	-8.35
MoO_2	-588.9	-764.4	3.61	-1.94
RuO_2	-305.0	-746.3	3.34	-1.94
RuO_4	-239.3	-746.3	7.45	-27.59
Rh_2O_3	-343.0	-741.1	6.46	4.47
PdO	-85.4	-735.6	6.28	10.88
Ag_2O	-31.1	-721.5	-3.36	17.29
CdO	-258.4	-737.5	-2.62	10.88
La_2O_3	-1793.7	-772.4	-7.54	4.47
HfO_2	-1144.7	-790.9	-4.58	-1.94
Ta_2O_5	-2046.0	-786.0	-1.83	-8.35
WO_2	-589.7	-772.8	12.01	-1.94
WO_3	-842.9	-772.8	-3.81	-14.77
Re_2O_7	-1240.1	-756.8	-5.93	-21.18
OsO_4	-394.1	-745.9	-2.70	-27.59
IrO_2	-274.1	-741.9	0.79	-1.94
HgO	-90.8	-724.0	-5.65	10.88

[a] Formation enthalpies for the oxides adopted from Lide R. D. (ed.), CRC Handbook of Chemistry and Physics, Internet Version, 2005 [33]; [b] Formation enthalpies for the metal doped

$M_{0.0625}V_{0.9375}O_2$; [(c)] Decomposition enthalpies for $M_{0.0625}V_{0.9375}O_2$; [(d)] Decomposition entropies for $M_{0.0625}V_{0.9375}O_2$; (e) adopted from reference [42].

Table 2. Equilibrium free energies, bulk moduli and their derivatives with to pressure, lattice parameters, and Fermi energies of the $M_{0.0625}V_{0.9375}O_2$ (the DFT calculations are carried with spin-polarization, and the lattice parameters are scaled to four units of $M_{0.0625}V_{0.9375}O_2$)

Dopants	U_0 (eV)	B_0 (GPa)	B_0'	V_0 (Å^3)	a (Å)	b (Å)	c (Å)	β (deg)	E_f (eV)
Sc	-22.6605	216	3.85	124.93	5.4587	4.5355	6.0738	123.815	3.22
Ti	-22.7590	242	2.40	123.80	5.4421	4.5174	6.0644	123.860	3.22
V	-22.5242	226	4.15	123.57	5.4420	4.5053	6.0775	123.971	3.53
Cr	-22.6617	225	4.41	123.14	5.4306	4.5055	6.0671	123.953	3.58
Mn	-22.5534	226	4.11	122.89	5.4275	4.5065	6.0531	123.900	3.52
Fe	-22.4315	173	3.50	121.14	5.4026	4.4775	6.0389	123.976	3.62
Co	-22.3004	206	5.34	122.78	5.4268	4.5160	6.0220	123.697	3.53
Ni	-22.1758	222	4.41	122.65	5.4247	4.5021	6.0497	123.886	3.28
Cu	-21.9920	204	5.72	123.57	5.4393	4.5221	6.0406	123.732	3.18
Zn	-21.9690	219	3.50	124.12	5.4484	4.5280	6.0508	123.747	3.13
Y	-22.6433	163	6.42	127.49	5.4956	4.5601	6.1331	123.948	3.20
Zr	-22.8532	229	3.62	125.76	5.4700	4.5363	6.1104	123.958	3.22

Nb	-22.8751	222	4.24	125.57	5.4690	4.5418	6.0840	123.806	3.40
Mo	-22.7787	215	3.39	125.73	5.4720	4.5482	6.0737	123.719	3.63
Ru	-22.4885	292	3.50	123.67	5.4395	4.5096	6.0801	123.981	4.21
Rh	-22.3088	227	4.19	124.09	5.4449	4.5154	6.0882	123.999	3.41
Pd	-22.1206	235	3.29	124.08	5.4452	4.5170	6.0810	123.942	3.21
Ag	-21.8281	214	5.02	124.93	5.4581	4.5214	6.1091	124.036	3.10
Cd	-21.8733	260	3.50	125.50	5.4679	4.5362	6.0983	123.924	3.20
La	-22.4872	197	3.50	130.30	5.5369	4.5878	6.1880	123.973	3.47
Hf	-22.9928	227	4.00	125.38	5.4647	4.5324	6.1015	123.934	3.20
Ta	-23.0616	223	4.25	125.40	5.4664	4.5387	6.0841	123.827	3.45
W	-22.9966	209	5.62	125.67	5.4692	4.5426	6.0844	123.761	3.55
Re	-22.7931	189	6.26	125.60	5.4701	4.5445	6.0750	123.728	4.03
Os	-22.6069	249	3.50	124.43	5.4519	4.5188	6.0880	123.944	4.25
Ir	-22.4155	234	3.50	124.61	5.4531	4.5199	6.0990	124.009	3.83
Pt	-22.2149	190	3.50	125.44	5.4653	4.5331	6.1032	123.943	3.28
Au	-21.8751	220	4.52	125.05	5.4613	4.5193	6.1215	124.142	3.61

Hg	-21.6898	211	3.27	126.75	5.4833	4.5507	6.1285	124.012	3.31

Table 3. Corresponding lattice parameters for the VO_2 (M_1) and VO_2 (R)

	VO_2 (M_1)	VO_2 (R)	Difference
V (Å^3)	118.07	118.44	0.37
β (deg)	122.6	122.1	-0.5
a or a' (Å)	5.375	5.383	0.008
b or b' (Å)	4.526	4.554	0.028
c or c' (Å)	5.753	5.712	-0.041

Table 4. A summary of the most studied dopants and their influences to transition temperatures

Dopants	T_c (undoped) (℃)	T_c (doped) (℃)	Doping level (at.%)	dT_c/dx (at.%/℃)	References
Mg^{2+}	68.0	54.0	7.0%	-2	[4]
Mg^{2+}	64.5	45.0	7.0%	-3	[11]
Ti^{4+}	66.9	66.9	3%	0	[44]
Cr^{3+}	57±1.6	61.9±2.2	6.5%	0.8	[8]
Cu^{2+}		56.5±7.5	2%	-5	[41]
Zn^{2+} & W^{6+}		44.0±6.2	10% + 10%	-2.4	[43]
ZrV_2O_7	58.1	59.1±14.2	2%	0.5	[45]
Nb^{5+}	58	35±3	2~3%	-7.8	[46]
Mo^{6+}	62.5	24.0	7.0%	-5.5	[6]
Mo^{6+}	64	41.0±1.0	2%	-11	[47]
Mo^{6+}	65	30.0	1.5%	-23	[48]
Sb^{3+}		61.5±10.5	3%		[49]
Ta^{5+}		48.0±1.2	3%		[50]
W^{6+}		54.1	0.54%	-23	[38]
F^-	66.0	35.0	2.9%	-10.6	[13]

ZnO:Al	58.2 ±22.0	38.1 ±14.5	[51]

Table 5. Short d_s and long d_l V-V distances and distortion angle δ of the V-V dimers in the transition metal M-doped VO_2 (M_1) calculated with spin-polarization

Dopants	δ (deg)	d_s (Å)	d_l (Å)
Sc	174.97	3.0328	3.0469
Ti	179.90	3.0290	3.0354
V	179.99	3.0385	3.0390
Cr	179.98	3.0334	3.0336
Mn	179.98	3.0259	3.0272
Fe	179.99	3.0184	3.0205
Co	179.97	2.8679	3.1542
Ni	179.99	3.0239	3.0258
Cu	179.75	2.9571	3.0835
Zn	179.96	3.0544	3.0560
Y	171.07	3.0724	3.0793
Zr	179.96	3.0544	3.0560
Nb	179.85	3.0367	3.0474
Mo	176.30	3.0082	3.0687
Ru	179.97	3.0396	3.0405
Rh	179.99	3.0435	3.0447
Pd	179.99	3.0404	3.0406
Ag	179.95	3.0543	3.0548
Cd	171.38	3.0558	3.0598
La	162.45	3.1246	3.1367

Hf	179.95	3.0504	3.0511
Ta	179.93	3.0416	3.0425
W	178.33	3.0284	3.0566
Re	179.39	3.0258	3.0493
Os	180.00	3.0438	3.0442
Ir	179.99	3.0489	3.0501
Pt	179.98	3.0514	3.0518
Au	179.97	3.0607	3.0608
Hg	170.19	3.0728	3.0782